Influence on Structural Loading of a Wave Energy Converter by Controlling Variable-Geometry Components and the Power Take-Off

Preprint

Salman Husain,[1] Jacob Davis,[2] Nathan Tom,[1]
Krish Thiagarajan,[2] Cole Burge,[3] and Nhu Nguyen[2]

1 National Renewable Energy Laboratory
2 University of Massachusetts Amherst
3 University of Washington

Presented at ASME 2022 41st International Conference on Ocean, Offshore and Arctic Engineering (OMAE2022)
Hamburg, Germany
June 5–10, 2022

NREL is a national laboratory of the U.S. Department of Energy
Office of Energy Efficiency & Renewable Energy
Operated by the Alliance for Sustainable Energy, LLC

This report is available at no cost from the National Renewable Energy Laboratory (NREL) at www.nrel.gov/publications.

Contract No. DE-AC36-08GO28308

Conference Paper
NREL/CP-5700-81883
June 2022

Influence on Structural Loading of a Wave Energy Converter by Controlling Variable-Geometry Components and the Power Take-Off

Preprint

Salman Husain,[1] Jacob Davis,[2] Nathan Tom,[1]
Krish Thiagarajan,[2] Cole Burge,[3] and Nhu Nguyen[2]

1 National Renewable Energy Laboratory
2 University of Massachusetts Amherst
3 University of Washington

Suggested Citation
Husain, Salman, Jacob Davis, Nathan Tom, Krish Thiagarajan, Cole Burge, and Nhu Nguyen. 2022. *Influence on Structural Loading of a Wave Energy Converter by Controlling Variable-Geometry Components and the Power Take-Off: Preprint*. Golden, CO: National Renewable Energy Laboratory. NREL/CP-5700-81883. https://www.nrel.gov/docs/fy22osti/81883.pdf.

NREL is a national laboratory of the U.S. Department of Energy
Office of Energy Efficiency & Renewable Energy
Operated by the Alliance for Sustainable Energy, LLC

This report is available at no cost from the National Renewable Energy Laboratory (NREL) at www.nrel.gov/publications.

Contract No. DE-AC36-08GO28308

Conference Paper
NREL/CP-5700-81883
June 2022

National Renewable Energy Laboratory
15013 Denver West Parkway
Golden, CO 80401
303-275-3000 • www.nrel.gov

NOTICE

This work was authored in part by the National Renewable Energy Laboratory, operated by Alliance for Sustainable Energy, LLC, for the U.S. Department of Energy (DOE) under Contract No. DE-AC36-08GO28308. Funding provided by U.S. Department of Energy Office of Energy Efficiency and Renewable Energy Water Power Technologies Office. The views expressed herein do not necessarily represent the views of the DOE or the U.S. Government. The U.S. Government retains and the publisher, by accepting the article for publication, acknowledges that the U.S. Government retains a nonexclusive, paid-up, irrevocable, worldwide license to publish or reproduce the published form of this work, or allow others to do so, for U.S. Government purposes.

Cover Photos by Dennis Schroeder: (clockwise, left to right) NREL 51934, NREL 45897, NREL 42160, NREL 45891, NREL 48097, NREL 46526.

INFLUENCE ON STRUCTURAL LOADING OF A WAVE ENERGY CONVERTER BY CONTROLLING VARIABLE-GEOMETRY COMPONENTS AND THE POWER TAKE-OFF

Salman Husain[1], Jacob Davis[2], Nathan Tom[1], Krish Thiagarajan[2], Cole Burge[3], Nhu Nguyen[2‡]

ABSTRACT

Oceans are harsh environments and can impose significant loads on deployed structures. The deployment of wave energy converters (WECs) faces a design challenge with apparently contradictory goals. A WEC should be designed to maximize the energy absorbed while ensuring the operating wave condition does not exceed the failure limits of the device itself. Therefore, the loads endured by the support structure are a design constraint for the system. Adaptability to different sea states is, therefore, highly desirable. This work uses a WEC-Sim model of a variable-geometry oscillating wave energy converter (VGOSWEC) mounted on a support structure simulated under different wave scenarios. A VGOSWEC resembles a paddle pitching about a fixed hinge perpendicular to the incoming wave fronts. Therefore, the hinge experiences loads perpendicular to its axis as it maintains its position. The geometry of the VGOSWEC is varied by opening a series of controllable flaps on the pitching paddle when the structure experiences threshold loads. Because opening the flaps lets the waves transmit through the paddle, it is hypothesized that opening the flaps should result in load shedding at the base of the support structure. The load shedding is achieved by reducing the moments about the hinge axis. This work compares the hydrodynamic coefficients, natural periods, and response amplitude operators from completely closed to completely open configurations of the controllable flaps. The comparisons quantify the effects of letting the waves transmit through the VGOSWEC. This work shows that the completely open configuration can reduce the pitch and surge loads on the base of the support structure by as much as 80%. It was observed that at the paddle's resonance frequency, the loads on the structure increased substantially. This increase in loads can be mitigated by a rotational power take-off damping about the hinge axis. Changing the rotational power take-off damping was identified as an additional design parameter that can be used to control the loads experienced by the WEC's support structure.

1 Introduction

In recent years renewable energy devices have achieved design convergence for solar and wind, but the research community designing marine energy extraction devices is still exploring various wave energy converters (WECs). WEC designs range from devices that are axisymmetric, usually oscillating in heave, and asymmetric, usually oscillating in surge or pitch modes [1]. An axisymmetric WEC (e.g., the CorPower WEC [2]) is agnostic to the incoming wave direction but sacrifices a significant amount of energy that could otherwise be extracted in modes that are orthogonal to the primary oscillating mode, as discussed by Korde et al. in their discussion on terminator-type WECs [1].

Some notable examples of pitching WECs in terminator configuration include Salter's Duck, which extracts energy using the mode-coupling of the surge, heave, and pitch modes, and the free-floating sloped Interproject Service (IPS) buoy, which extracts energy by the mode-coupling of surge and heave [3, 4].

*[1]Salman Husain and Nathan Tom are with the Water Power Department, National Renewable Energy Laboratory, Golden, CO 80401, USA sal.husain@nrel.gov,nathan.tom@nrel.gov

†[2]Jacob Davis, Krish Thiagarajan Sharman, and Nhu Nguyen are with the Department of Mechanical and Industrial Engineering, University of Massachusetts Amherst, Amherst, MA 01003, USA jacrdavis@umass.edu, kthiagarajan@umass.edu, nvnguyen@umass.edu

‡[3]Cole Burge is with the Department of Mechanical Engineering, University of Washington, Seattle, WA 98195, USA coleburge@gmail.com

Terminator-type devices are usually suitable for near-shore deployment because the energy of the water particles increases in the horizontal direction as the waves approach the coast. The near-shore deployment of terminator-type WECs opens up the possibility of rigid support structures that can allow greater motion in the power take-offs (PTOs) and generate greater power compared to devices like the Reference Model 5 or the Langlee WEC [5].

The design workflow for a WEC is constrained by factors such as structural load and control. Therefore, WEC design requires robust support structures that can withstand extreme weather events. Adaptability to the wave loads on the structure is a critical design constraint that should be part of the WEC design process. Tom et al. discussed a variable-geometry oscillating surge wave energy converter (VGOSWEC), which was developed at the National Renewable Energy Laboratory (NREL) [6]. A VGOSWEC is an oscillating surge WEC (OSWEC) with controllable flaps to alter the device geometry, and thus the device hydrodynamics, to reduce loads on the WEC support structure [7]. The variable-geometry feature of the VGOSWEC expands the range of operable sea states. Kelly et al. simulated the performance of VGOSWEC devices at three different sites across the United States and assessed the load-shedding advantages of variable-geometry WEC designs [8]. Choiniere et al. developed a VGOSWEC that can reduce the loads on the supporting structure using controllable load-relief flaps on the VGOSWEC when a threshold loading is experienced [9]. Therefore, the variable geometry can help design better-informed control strategies in tandem with the PTO-based control.

The range of deployment sites can be further expanded by mounting VGOSWEC devices on a raised platform. Such design configurations have been researched for an OSWEC-type device. Burge et al. showed that mounting an OSWEC on a raised platform expands the number of available installation sites, with potentially higher energy yields [10]. They analyzed an OSWEC mounted on a raised platform and explored the effect of lowering pressure plates and changing the parameters of the supporting foundation to maximize performance at different operating conditions and wave climates [10].

The work presented here models a raised-platform-mounted VGOSWEC that emulates the model-scale tests completed at the University of Massachusetts Amherst. These tests were funded by the U.S. Department of Energy Office of Technology Transitions Technology Commercialization Fund Award [10–12]. The hypothesis for this work is to demonstrate that controllable flaps on a VGOSWEC reduce the loads experienced by the supporting raised platform. A WEC-Sim numerical model [13] is used to analyze the natural periods, response amplitude operators (RAOs), and loads on the support structure to determine if the hypothesis holds true.

2 Description of a Raised VGOSWEC

The raised VGOSWEC considered in this study is a two-body system, as illustrated in Figure 1. The device comprises a paddle of width 0.4 m and height 0.5 m that is mounted on a monopile such that the paddle is free to pitch about an axle running through the paddle near its bottom surface. The monopile is rigidly attached to the bottom surface of the wave tank. The paddle has a series of four flaps that can be configured to be: (i) completely closed, (ii) partially open at some predefined angle, and (iii) completely open. The objective of the configurable flaps is to reduce the surface pressure exerted on the VGOSWEC to reduce the incoming excitation forces on the paddle so that the loads acting on the monopile are reduced. A rotary PTO is implemented using a spring with no damping. Table 1 shows the physical parameters of the paddle used in the numerical models that follow. The pertinent equations of motion are discussed in Section 2.1, followed by the development of a numerical time-domain simulation using WEC-Sim in Section 2.2.

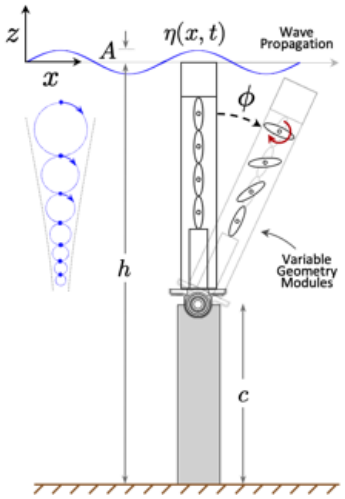

FIGURE 1. Schematic representation of the VGOSWEC, where h is the water depth, c is the height of the support structure, η represents the wave elevation A is wave amplitude, and ϕ represents the pitch angle. The flaps are controllable such that the 0° configuration represents the completely closed configuration, and the 90° configuration represents the completely open configuration.

2.1 VGOSWEC Equation of Motion, Surge Foundation Force, and Pitch Foundation Moment

The dynamics of the two-body system simulated here are mutually coupled. The equations of motion for N coupled bodies will comprise $6N \times 6N$ modes for the phenomena affected by the floating body and $6N \times 1$ modes for the incident excita-

Property	Variable	Value	Unit
Width	w	0.4	m
Height	H_p	0.5	m
Thickness	t	0.076	m
Paddle geometry	-	-	-
	Cross section	ellipse	-
	Number	4	-
	Paddle length	0.349	m
	Paddle cord	0.076	m
	Paddle thickness	19	mm
Body mass	m	6.30	kg
Displaced volume	$\forall$	7395	cm^3
Center of gravity*	r_g	0.274	m
Center of buoyancy*	r_b	0.293	m
Moment of inertia	I_{55}	0.962	kg m^2
Foundation geometry	-	cylindrical	-
Foundation radius	r_f	0.05	m
External springs	C_{ext}	6.57	kg m^2 s^{-2}

TABLE 1. Geometric and Inertial Properties of the VGOSWEC. * denotes measurements from the hinge.

tion force because it is the input to the system independent of the body response and its couplings. Therefore, the radiation damping, added mass, and hydrostatic force matrices in this case will be 12×12 while the excitation force coefficient matrix will be 12×1. In the discussion that follows, the modes are ordered as surge, sway, heave, roll, pitch, and yaw. Modes 1–6 represent the paddle's modes, and modes 7–12 correspond to the monopile. Therefore, the surge mode for the paddle will be represented as the ordered pair, $1,1$, the surge mode of the monopile will be represented as $7,7$, and the coupled modes will be represented as an ordered pair made up from a combination of modes 1–6 and 7–12. The notations for the rest of the paper will have two-digit ordered pair subscripts representing the corresponding mode. The auto-coupled terms (i.e., the body-only modes such as surge, heave, and pitch) make up the diagonal terms in the $6N \times 6N$ matrices while the coupled modes make up the corresponding off-diagonal terms.

As shown in [7], the VGOSWEC linear pitch equation of motion about the hinge can be modeled in the frequency domain as

$$\frac{\xi_{5,5}}{A} = \frac{E_{5,5}}{\left[C_{5,5} - \omega^2 \left(I_{5,5} + \mu_{5,5}\right)\right] + i\omega\left[\lambda_{5,5} + \lambda_g\right]} \tag{1}$$

where A is the amplitude and ω the angular frequency of the incident wave, $\xi_{5,5}$ is the complex pitch displacement amplitude, $E_{5,5}$ is the complex pitch excitation torque per unit wave amplitude, C_{55} is the pitch restoring coefficient, I_{55} is the pitch mass moment of inertia, μ_{55} is the pitch radiation added moment of inertia, λ_{55} is the pitch radiation damping, and λ_g is the linear, rotational PTO damping. The hinge that the VGOSWEC rotates about will have to withstand surge forces due to the surge excitation force on the VGOSWEC and from the radiation surge-pitch coupling forces [7] such that

$$E_{r1,1} + E_{1,1} = \left[-\omega^2 \mu_{1,5} + i\omega\lambda_{15}\right] \frac{\xi_{5,5}}{A} \tag{2}$$

where $E_{r1,1}$ is the hinge reaction force per unit wave amplitude in the surge mode, $\mu_{1,5}$ is the surge-pitch radiation added mass, λ_{15} is the surge-pitch radiation damping, and $E_{1,1}$ is the surge-wave excitation force, per unit wave amplitude. The monopile foundation is assumed to be sufficiently rigid to prevent any oscillatory motion, thereby eliminating any radiation forces from the foundation. From this approximation, a summation of the surge forces at the base of the monopile foundation can be modeled as

$$-E_{r1,1} + E_{7,7} + E_{r7,7} = 0 \rightarrow E_{r7,7} = E_{r1,1} - E_{7,7} \tag{3}$$

where $E_{r7,7}$ is the foundation reaction force in the surge mode. Substituting Equation (2) in Equation (3) and rearranging,

$$E_{r7,7} = -E_{1,1} - E_{7,7} + \left[-\omega^2 \mu_{1,5} + i\omega\lambda_{1,5}\right] \frac{\xi_{5,5}}{A} \tag{4}$$

where $E_{7,7}$ is the surge excitation force on the monopile foundation. Equation (4) shows that the foundation reaction force in surge mode has contributions from the surge excitation force on the VGOSWEC, the surge-pitch radiation force on the VGOSWEC, and the surge excitation force on the monopile.

The moment at the base of the monopile foundation will also include contributions from the excitation loads on the centers of gravity of the paddle and the monopile, along with the VGOSWEC radiation forces, such that

$$-E_{r1,1}c + E_{7,7}\frac{c}{2} + E_{9,9} + E_{r9,9} = 0 \tag{5}$$

$$\rightarrow E_{r9,9} = E_{r1,1}c - E_{7,7}\frac{c}{2} - E_{9,9} \tag{6}$$

where $E_{9,9}$ is the pitch-wave excitation moment on the monopile foundation and $E_{r9,9}$ is the foundation reaction moment in the pitch mode. Equation 6 can be expanded using Equation (4)

such that the contributions to the monopile pitch reaction moment, $E_{r9,9}$, can be expressed as

$$E_{r9,9} = \left(-E_{1,1} + \left[-\omega^2\mu_{15} + i\omega\lambda_{15}\right]\frac{\xi_{5,5}}{A}\right)c - E_{7,7}\frac{c}{2} - E_{9,9} \quad (7)$$

$$E_{r9,9} = -E_{1,1}c + \left[-\omega^2\mu_{15} + i\omega\lambda_{15}\right]\frac{\xi_{5,5}}{A}c - E_{7,7}\frac{c}{2} - E_{9,9} \quad (8)$$

$$E_{r9,9} = -E_{9,9} - \frac{c}{2}\left(2E_{1,1} + E_{7,7}\right) + \left[-\omega^2\mu_{15} + i\omega\lambda_{15}\right]\frac{\xi_{5,5}}{A}c \quad (9)$$

2.2 VGOSWEC Hydrodynamics Coefficients

A floating body in water experiences the excitation force (Froude-Krylov force), the diffraction force, the hydrostatic force, and the radiation force. The diffraction and the radiation problem is solved by calculating the frequency-dependent hydrodynamic coefficients to write the frequency-domain equations of motion. The time-domain models discussed in Section 3 are then developed using the impulse response functions calculated using the Fourier transforms of the frequency-dependent terms.

The hydrodynamic coefficients for this paper were calculated using the boundary-element-method-based commercial software WAMIT. The hydrodynamic and hydrostatic forces are calculated by discretizing the body geometry in bounded panels. The surface integrals of the pressure due to the incoming wave manifests as the excitation force (or the dynamic Froude-Krylov force), and the subsequent scattered wave diffracted by the body manifests as the diffraction force. The hydrostatic force represents the buoyancy force calculated as the surface integral of the pressure exerted on the body due to water's reaction force to the body's weight force, and the radiation force is the surface integral of the pressure exerted on the body as a reaction to the radiated wave field generated by the body when it is in motion.

The hydrodynamic coefficients for five VGOSWEC configurations ($0^\circ, 10^\circ, 20^\circ, 45^\circ$, and 90°) are shown in Figure 2(a)–2(d). The VGOSWEC hydrodynamic coefficients decrease as the paddle is opened from the 0° configuration to the 90° configuration. Also, the normalized hydrodynamic coefficients in pitch mode were found to be an order of magnitude smaller than those in surge mode. Figure 2(a)–2(d) compares the VGOSWEC surge and pitch hydrodynamic coefficients for (i) the paddle at all geometric configurations and (ii) the monopile.

Notice that the peaks of the lobes align obliquely for all the cases in Figure 2(a)–2(d) around 7 rad/s (0.897 s wave period). This indicates the effect that the wave-tank walls or the wave-tank geometry and depth may have on the hydrodynamic coefficients. The WAMIT model included the sidewalls and the bottom surface of the wave tank to emulate the wave-tank experimental setup as closely as possible with this approach. Although the boundary element method calculations in WAMIT modeled the wave tank's sidewalls, it did not model the walls parallel to the hinge axis. This could potentially introduce some divergence from experimental results.

It can be observed that there is a significant decrease in the hydrodynamic coefficients from the 0° configuration to all of the other configurations. Recall that the hydrodynamic coefficients are calculated as the surface integrals of the corresponding wave potential field. This drop can be attributed to the drop in the pressure exerted on the paddle as the flaps are opened. The hydrodynamic coupling between the paddle and the monopile introduced this effect onto the hydrodynamic coefficients of the monopile as well. Since the hydrodynamic forces are calculated using the hydrodynamic coefficients, it can be hypothesized that the time-domain modeling will show similar patterns in the loads exerted on the foundation (i.e., reducing in magnitude as the flaps are opened to the fully open 90° configuration).

The loads experienced at the foundation will have their moment arm from the foundation to the centers of gravity of the paddle and monopile, so the moments at the foundation will have contributions from the surge and pitch loads. The hydrodynamic coefficients are calculated at the body's center of gravity, whereas the equations in Section 2.1 are calculated at the hinge, about which the paddle oscillates in pitch mode. The equations in Section 2.1, therefore, need the appropriate transpositions to the hinge.

3 WEC-Sim VGOSWEC Model Development

WEC researchers typically use the Cummins equation to model the WEC dynamics in the time domain [14–16]. The WEC model was simulated using WEC-Sim, which is a time-domain solver for WECs developed jointly by NREL and Sandia National Laboratories [13]. The hydrodynamic coefficients were postprocessed using the 'BEMIO' utility that is part of the WEC-Sim suite. The hydrodynamic coefficients, their corresponding impulse response functions, and relevant physical parameters were saved as data structures in an '*.h5' file and a MATLAB data file in the '*.mat' format. The WEC-Sim model then implemented the Cummins equation using a customized library of Simulink blocks in the Simscape multibody library. The PTO was modeled using a rotational PTO block from the WEC-Sim library. The PTO stiffness and damping values were defined such that they were consistent with the planned experiments [12]; the PTO stiffness was set at $K_{PTO} = 6.57$ N/m, and the PTO damping was set at $C_{PTO} = 0$ N·s/m. The damping was set at 0 to investigate the effect of changing the geometric configuration alone. The effect of changing PTO damping is discussed in Section 5.

3.1 Free-Decay WEC-Sim Simulations

Free-decay simulations were conducted to determine the natural frequency, ω_n, and damping ratio, ζ, of the VGOSWEC in different geometric configurations. The natural frequencies

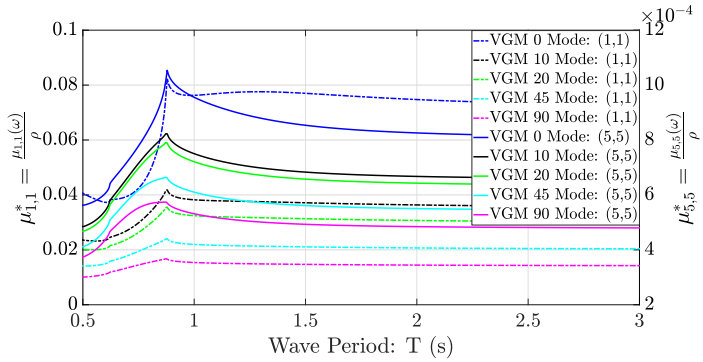

(a) The comparison of surge (left vertical axis) and pitch (right vertical axis) added mass coefficients for the paddle.

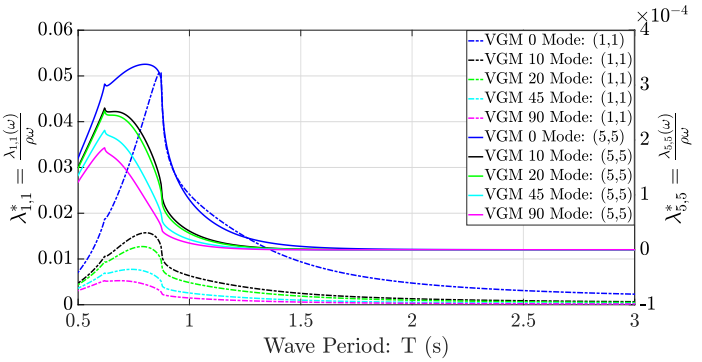

(b) The comparison of surge (left vertical axis) and pitch (right vertical axis) normalized radiation damping coefficients for the paddle.

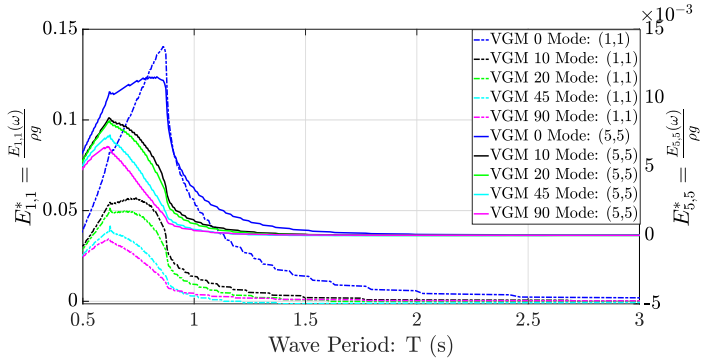

(c) The comparison of surge (left vertical axis) and pitch (right vertical axis) normalized excitation force coefficients for the paddle.

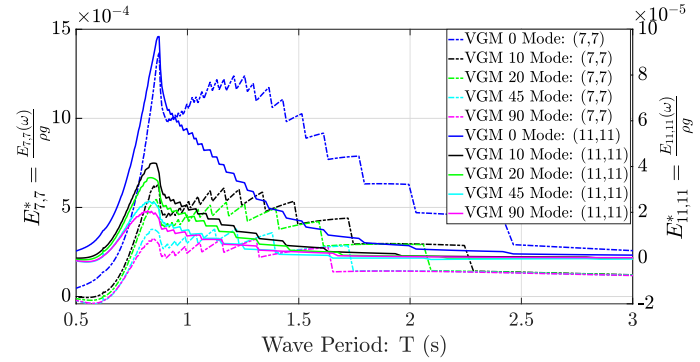

(d) The comparison of surge (left vertical axis) and pitch (right vertical axis) normalized excitation force coefficients for the monopile.

FIGURE 2. The comparison of normalized hydrodynamic coefficients.

Geometric Configuration	ω_n [rad/s]	T_s [s]	$\zeta \times 10^{-4}[-]$
VGM 0	1.07	5.86	5.8
VGM 10	1.46	4.29	4.3
VGM 20	1.57	4.01	4.1
VGM 45	1.84	3.42	3.5
VGM 90	2.10	2.99	3.2

TABLE 2. Natural frequency for each VGOSWEC geometric configuration measured from free-decay simulations.

for each geometry were obtained by performing a fast Fourier transform (FFT) on the time history of the free-decay pitch responses. Table 3.1 shows that the natural frequency increases as the flaps on the VGOSWEC are opened, indicating that the net added mass moment about the hinge has been reduced. The decrease in added mass emboldens the hypothesis that the opening of the flaps of the VGOSWEC decreases the structural loading on the foundation. The natural frequency of the VGOSWEC in different geometric configurations was determined by using the frequencies corresponding to resonant peaks in the FFT. Figure 3 shows the FFTs for a free-decay test when the initial displacement is 10.4°.

Table 3.1 also shows the damping ratio, ζ, calculated using the log-decrement method. The damping ratio decreases by $\approx 50\%$ from the 0° configuration to the 90° configuration. This corroborates the decline in radiation damping coefficients in Figure 2(c).

4 Effects of Varying the Geometry

This section would discuss the effect of varying the geometry for different values of PTO damping. This section would first show the bounding cases of zero PTO damping and infinite PTO damping, followed by a sweep of PTO damping values.

4.1 At Zero PTO Damping

The VGOSWEC geometry was varied such that the flaps were completely closed in the 0° configuration to completely open in the 90° configuration, with results shown in Figures 5–7. Figures 5–7 show that although the pitch displacements increase as the flaps of the VGOSWEC are opened, the structural loads

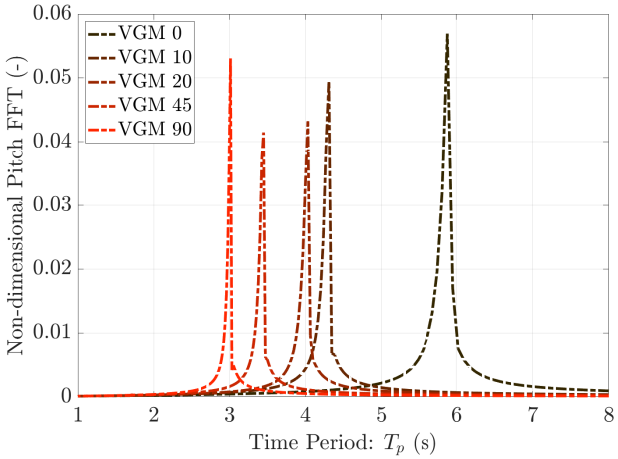

FIGURE 3. The nondimensionalized FFT for the pitch displacements, where the nondimensional pitch displacements were $\xi_5{}^* = \frac{\xi_5}{ka}$. The frequency corresponding to the peaks represents the natural frequencies.

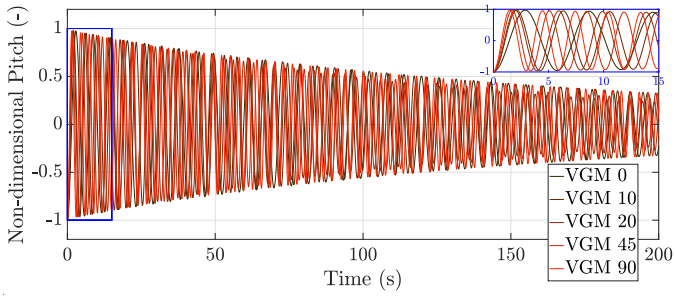

FIGURE 4. The nondimensionalized time series for the pitch displacements.

experienced at the bottom of the foundation decrease between the time periods 0–2 s. Note that the VGM 90 configuration has its natural frequency at a wave period of 2.99 s. These loads are exacerbated because there is greater motion, and the phase difference between motion and excitation increases. Tom et al. (2017) show that the resonance condition shifts the amplitude response relative to the wave phase, which causes an amplification of loads on the foundation [17].

4.2 At Infinite PTO Damping

As the PTO damping coefficient, λ_g, approaches infinity, the VGOSWEC will essentially be locked in place atop the foundation, and the only forces and moments on the foundation will be from the wave excitation forces and moments. This follows from Equation 1, where as the PTO damping coefficient approaches infinity the pitch RAO approaches 0 ($\lambda_g \to \infty \implies \xi \to 0$). Recall that Equation 4 gives the relation for the reaction loads on

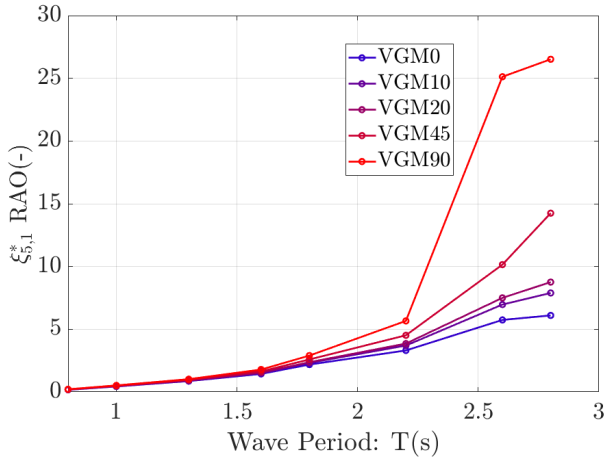

FIGURE 5. Comparison of nondimensional pitch displacements across different geometric configurations of the VGOSWEC. The pitch displacements were nondimensionalized using the wave number k and wave amplitude a such that the non-dimensional Pitch $RAO^* = \frac{\xi_5}{ka}$. The PTO damping for this case was set to zero.

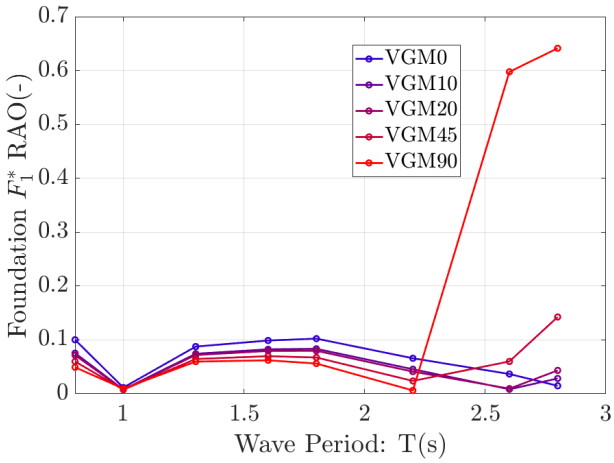

FIGURE 6. Comparison of nondimensional surge force across different geometric configurations of the VGOSWEC, where $F_1^* = \frac{F_1}{\frac{1}{2}\rho g w H_p a}$. The PTO damping for this case was set to zero.

the foundation; the right side of the equation has contributions from the excitation loads. The configurations with higher excitation load hydrodynamic coefficients will lead to the highest loads on the foundation. Therefore, since the 0° configuration has the largest wave excitation coefficients, it experiences the largest loads at the base of the foundation when the connection between the VGOSWEC and the foundation is rigid, and the paddle is locked in place as shown in Figures 8–10. However, locking the 90° configuration leads to the lowest surge force and pitch

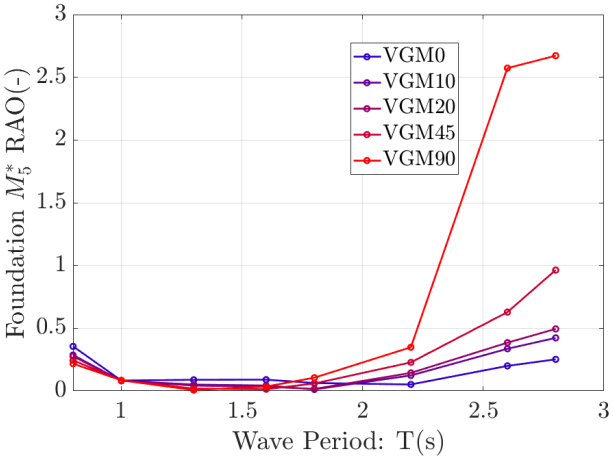

FIGURE 7. Comparison of nondimensional pitch moment on the foundation across different geometric configurations of the VGOSWEC, where $M_5^* = \frac{F_5}{\frac{1}{6}\rho g w H_p^2 a}$. The PTO damping for this case was set to zero.

moment on the foundation compared to when the other configurations are held fixed.

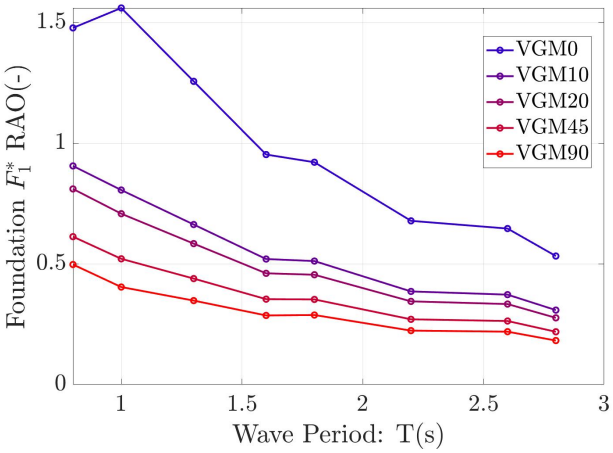

FIGURE 8. Surge force on the foundation at infinite PTO damping.

5 Effects of Varying the PTO Damping

Additional simulations were performed by varying the PTO damping coefficients from 0.5 N·s/m to 5.0 N·s/m to observe their effect on pitch displacement and foundation loads corresponding to the different geometric configurations. Figures 11–15 show the effect of varying PTO damping on the nondimensionalized pitch displacement of the paddle, the nondimensionalized surge force, and the pitch moment on the foundation.

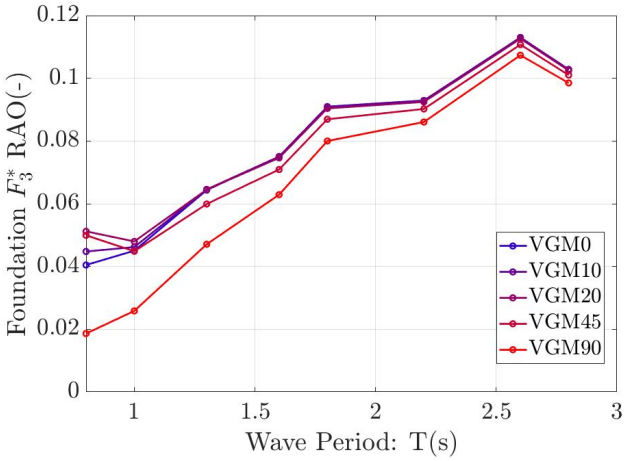

FIGURE 9. Heave force on the foundation at infinite PTO damping.

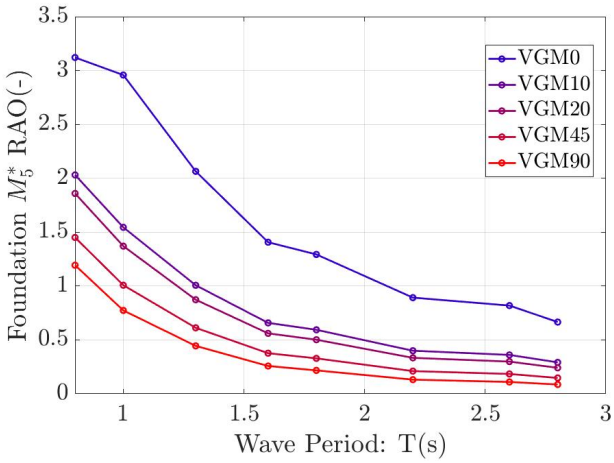

FIGURE 10. Pitch moment on the foundation at infinite PTO damping.

The effect on the nondimensionalized average power is shown in Figure 16(a) and 16(b). When the PTO damping coefficient was increased, the surge force and pitch moment measured at the base of the foundation also increased, with the largest loading occurring for the 0° configuration. The power plots in Figure 16(a) and 16(b) show that the PTO generated the highest power from the 0° configuration with the largest damping coefficients. Therefore, the higher PTO damping coefficients and the 0° configuration can be used as an optimum, and it is likely that the largest damping value for power production while opening the flaps can achieve the desired load shedding by reducing the forces and moments on the foundation.

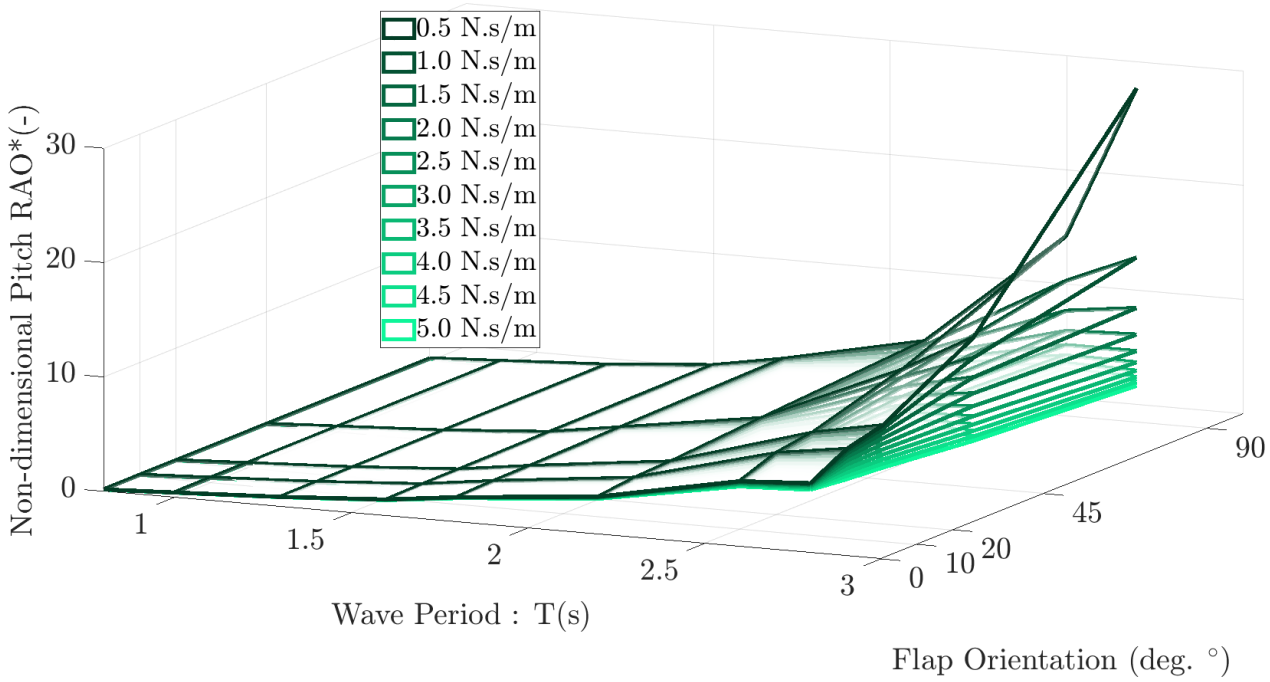

FIGURE 11. Comparison of normalized pitch displacement when the PTO damping is swept from 0.5 N·s/m to 5.0 N·s/m.

In Figure 16(a) and 16(b), the average power is normalized by dividing the average power produced by the paddle (using the PTO force and the oscillation velocity) by the average incident power. The average incident power can be expressed as

$$\bar{P}_I = \bar{e} v_g, \text{ where } \bar{e} = \frac{1}{2}\rho g A^2(\omega) \text{ and, } v_g = \frac{1}{2}\frac{\omega}{k}\left(1 + \frac{2kh}{\sinh 2kh}\right) \tag{10}$$

where $\bar{e}$ is the energy density, and v_g is the group velocity [1, 16, 18–20]. The nondimensionalized average power is then calculated using

$$\bar{P}^* = \frac{\bar{P}}{\bar{P}_I} \tag{11}$$

The 90° configuration case oscillates significantly less than the 0° configuration case for the same PTO damping value while experiencing the same wave conditions.

The WEC-Sim results demonstrate that combined control of the flap orientation and the PTO damping coefficient can help limit loading on the supporting foundation design, which is expected to reduce the required materials and drive the cost of energy down.

6 Discussion

A WEC needs to acclimatize to the harsh marine environment and weather events such as hurricanes and tsunamis. The structural loading imposed by the wave climate poses an existential challenge if the WEC structure fails to survive such conditions. Additionally, the fatigue due to structural loading over time also constrains the service life of the WEC. The VGOSWEC design modeled here can control the transmission of the incoming waves through the WEC structure, thereby extending the service life and reducing maintenance costs. The hydrodynamic coefficients calculated using WAMIT showed that the hydrodynamic coefficients decreased in magnitude as the flaps were opened. This decline can be attributed to the increased transmission of the incoming waves, thereby reducing the pressure experienced by the WEC structure.

Figures 12 and 13 show the effect of changing the PTO damping on the surge forces and pitch moment experienced at the base of the foundation. The structural loading trends support the hypothesis that opening the flaps of the VGOSWEC reduces the structural loads at the base of the foundation. The load-shedding hypothesis was also corroborated when the PTO damping was increased to infinity, such that the VGOSWEC was held fixed. Observe the reduction in the hydrodynamic loading at the base (Figures 8–10) of the supporting foundation as the VGOSWEC flaps are opened from the completely closed (90°) configuration

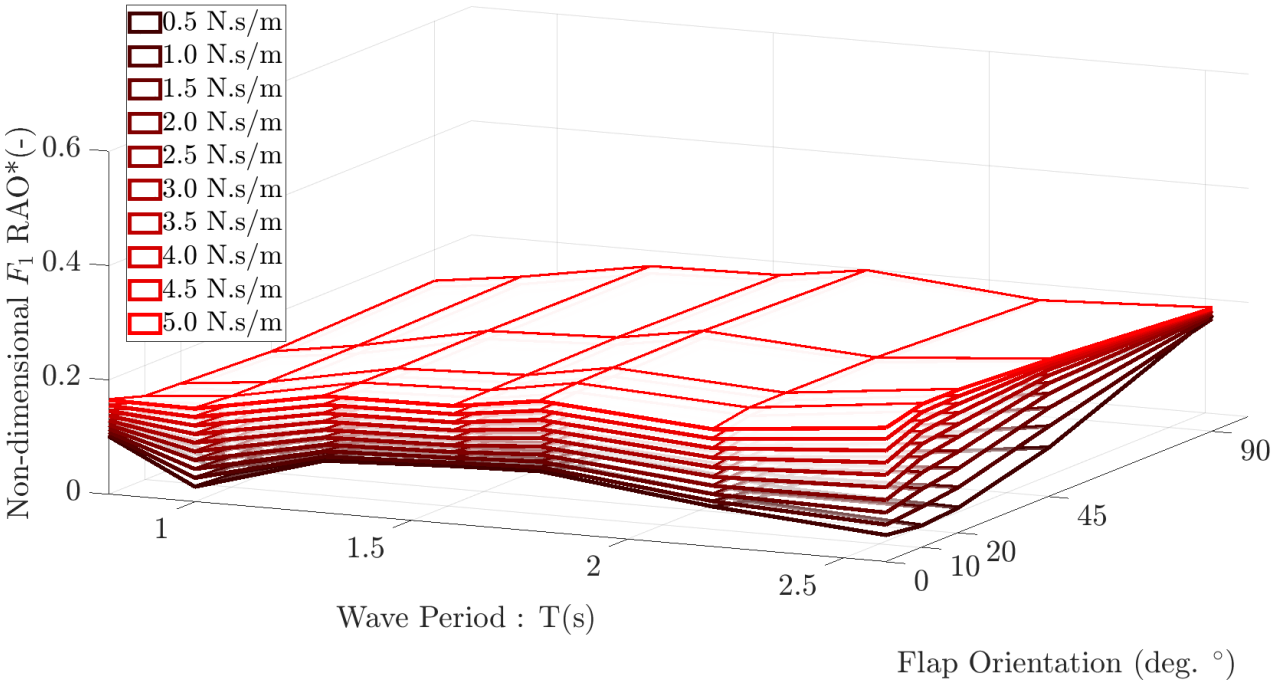

FIGURE 12. Comparison of normalized surge force on the foundation when the PTO damping is swept from 0.5 N·s/m to 5.0 N·s/m.

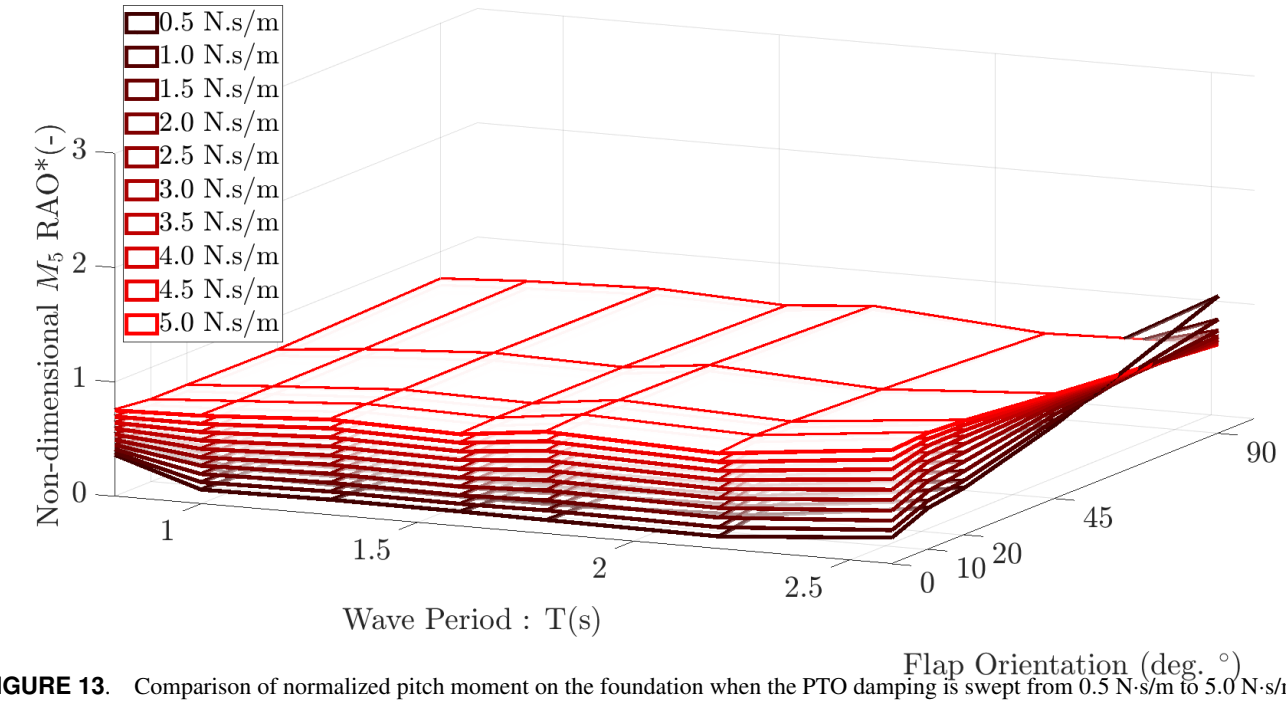

FIGURE 13. Comparison of normalized pitch moment on the foundation when the PTO damping is swept from 0.5 N·s/m to 5.0 N·s/m.

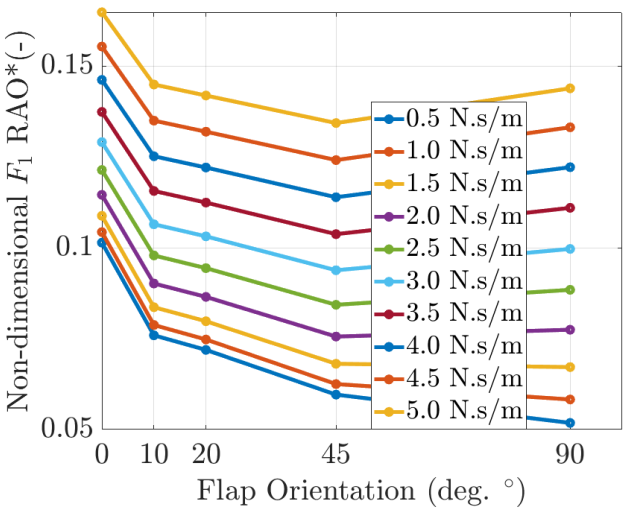

FIGURE 14. Comparison of normalized surge force on the foundation when the PTO damping is swept from 0.5 N·s/m to 5.0 N·s/m at a wave period of 0.8 s.

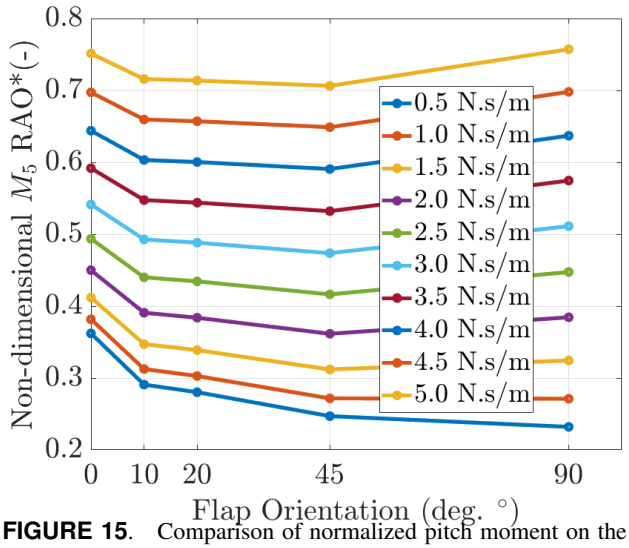

FIGURE 15. Comparison of normalized pitch moment on the foundation when the PTO damping is swept from 0.5 N·s/m to 5.0 N·s/m at a wave period of 0.8 s.

to the completely open (0°) configuration. These trends satisfied the load-shedding motivation for varying the geometry of the VGOSWEC. Figures 14 and 15 show the foundation loads as the PTO damping is varied from 0.5 N.s/m to 5.0 N.s/m at a wave period of 0.8 s. At shorter waves and at lower PTO damping values, the load shedding for the 90° configuration is highest.

However, as the PTO damping is increased, the foundation loads for the 90° configuration increase with respect to the 45° configuration (while still lower than for the more closed configurations). This apparently anomalous behavior could be attributed to the resonance-induced increase in oscillations and foundation loads. The free-decay tests, completed using WEC-Sim, were used to determine the natural frequency of the VGOSWEC (when allowed to freewheel by setting the PTO damping to zero) in different geometric configurations. The natural frequency of each geometric configuration explains the increase in oscillations and loads in longer wave periods. Note that from the free-decay cases, the resonance period of the 90° configuration was lower than that of the other configurations (see Table 3.1). This causes an increase in loads for the 90° configuration at wave periods closer to its natural period.

The comparison of foundation loads for a shorter wave period (0.8 s in Figures 14 and 15) illustrates that the load shedding is highest for the 90° configuration for lower PTO damping coefficients; this trend is reversed for longer waves that are closer to the 90° configuration's natural period, as shown in Figures 12 and 13. However, overall, the foundation loads are lower for the completely open 90° configuration when compared to the completely closed 0° configuration.

The comparison of average power generated by the PTO is shown in Figure 16(b). Notice as the PTO damping coefficient, C_{PTO}, is increased, the average power also increases. This indicates that higher generated power corresponds to the increase in foundation loads. This trade-off between power produced and foundation loads can be an important consideration for control. Further investigation of the PTO parameters could help balance the power generation objectives and the need for load shedding in extreme conditions.

7 Conclusions

The time-domain models developed in this work using WEC-Sim provided valuable insights into the dynamics of the VGOSWEC. The versatility to quantify loading at various locations on the WEC geometry can inform the design process before the logistically intensive experimental testing is conducted. This works shows that the loads experienced at the foundation of the support structure are related to the VGOSWEC oscillations in addition to the prevailing wave climate. The time-domain simulations corroborated the hypothesis that having controllable flaps that allow transmission of water can significantly reduce the loads on the supporting structure. Additionally, the loads experienced at the foundation of a VGOSWEC are also affected by dynamic response characteristics at natural periods and PTO design parameters. Future work could investigate VGOSWEC designs that incorporate PTO design and control for load shedding. Future VGOSWECs could also incorporate adaptability to changes in wave directions. Nevertheless, the capability to adapt device geometry expands the sites and conditions in which the VGOSWEC can operate.

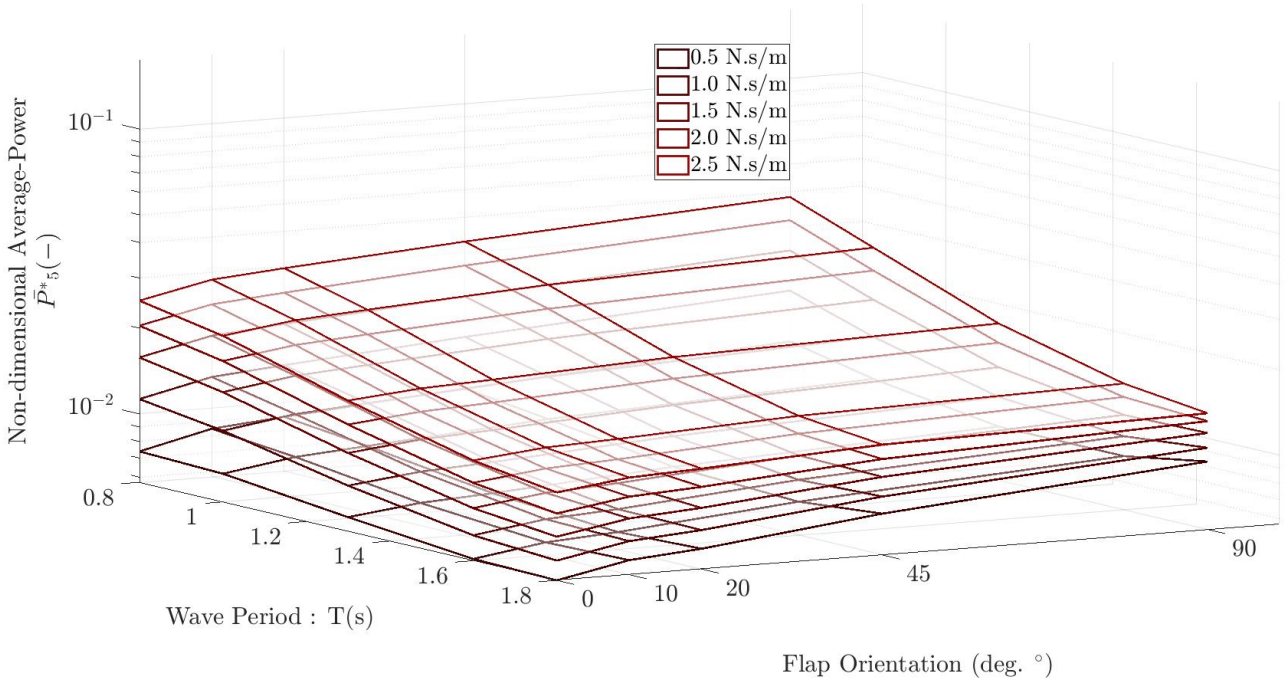

(a) $\bar{P}^*_5$ when the PTO damping is swept from 0.5 N·s/m to 2.5 N·s/m.

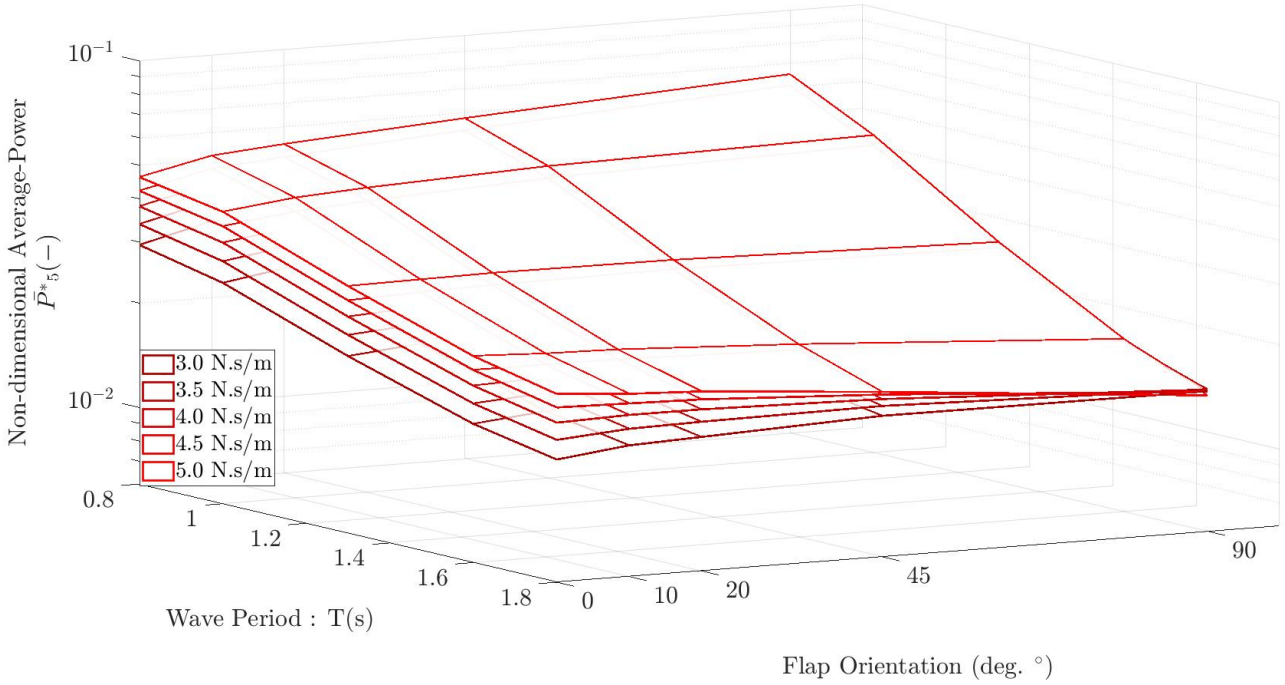

(b) $\bar{P}^*_5$ when the PTO damping is swept from 3.0 N·s/m to 5.0 N·s/m.

FIGURE 16. Comparison of normalized average power, $\bar{P}^*_5$.

ACKNOWLEDGMENT

This work was authored in part by the National Renewable Energy Laboratory, operated by Alliance for Sustainable Energy, LLC, for the U.S. Department of Energy (DOE) under Contract No. DE-AC36-08GO28308. Funding provided by the U.S. Department of Energy Office of Energy Efficiency and Renewable Energy Water Power Technologies Office. The views expressed in the article do not necessarily represent the views of the DOE or the U.S. Government. The U.S. Government retains and the publisher, by accepting the article for publication, acknowledges that the U.S. Government retains a nonexclusive, paid-up, irrevocable, worldwide license to publish or reproduce the published form of this work, or allow others to do so, for U.S. Government purposes.

REFERENCES

[1] Korde, U. A., and Ringwood, J., 2016. *Hydrodynamic Control of Wave Energy Devices*. Cambridge University Press, Sept.

[2] Todalshaug, J. H., Ásgeirsson, G. S., Hjálmarsson, E., Maillet, J., Möller, P., Pires, P., Guérinel, M., and Lopes, M., 2016. "Tank testing of an inherently phase-controlled wave energy converter". *International Journal of Marine Energy,* ***15***, Sept., pp. 68–84.

[3] Salter, S., 2016. "Wave energy: Nostalgic Ramblings, future hopes and heretical suggestions". *Journal of Ocean Engineering and Marine Energy,* ***2***(4), Nov., pp. 399–428.

[4] Parkin, P., Payne, G., and Taylor, J., 2003. "Numerical simulation and tank tests of the free0floating sloped ips buoy". *Fifth European Wave Energy Conference. University College Cork, 17020th september*.

[5] Yu, Y.-H., Li, Y., Hallett, K., and Hotimsky, C., 2014. "Design and Analysis for a Floating Oscillating Surge Wave Energy Converter". In Volume 9B: Ocean Renewable Energy, American Society of Mechanical Engineers, p. V09BT09A048.

[6] Tom, N., Lawson, M., Yu, Y.-H., and Wright, A., 2015. "Preliminary Analysis of an Oscillating Surge Wave Energy Converter with Controlled Geometry: Preprint".

[7] Kelly, M., Tom, N., Yu, Y.-H., Wright, A., and Lawson, M., 2021. "Annual performance of the second-generation variable-geometry oscillating surge wave energy converter". *Renewable Energy,* ***177***, pp. 242–258.

[8] Kelly, M., Tom, N., Yu, Y.-H., Wright, A., and Lawson, M., 2020. "Annual Performance of the Second-Generation Variable-Geometry Oscillating Surge Wave Energy Converter". *Renewable Energy*, Nov.

[9] Choiniere, M., Tom, N., and Thiagarajan, K. P., 2019. "Load shedding characteristics of an oscillating surge wave energy converter with variable geometry". *Ocean Engineering*.

[10] Burge, C., Tom, N., Thiagarajan, K., Davis, J., and Nguyen, N., 2021. "Performance Modeling of a Variable-Geometry Oscillation Surge Wave Energy Converter on a Raised FOUNDATION". p. 11.

[11] Nguyen, N., Davis, J., Thiagarajan, K., Tom, N., and Burge, C. "Optimizing power generation of a bottom-raised oscillating surge wave energy converter using a theoretical model". p. 9.

[12] Technology Commercialization Fund.

[13] Ruehl, K., Ogden, D., Yu, Y.-H., Keester, A., Tom, N., Forbush, D., and Leon, J., 2021. WEC-Sim v4.4, Oct.

[14] Cummins, W. E., Iiuhl, W., Uinm, A., and Cummins, W. E., 1962. The Impulse Response Function and Ship Motions. Tech. rep.

[15] Falnes, J., and Kurniawan, A., 2015. "Fundamental formulae for wave-energy conversion". *Royal Society Open*

Science, ***2***(3), Mar., p. 140305.
[16] Newman, J. N., 1977. *Marine hydrodynamics*. MIT Press, Cambridge, Mass.
[17] Tom, N. M., Yu, Y. H., Wright, A. D., and Lawson, M. J., 2017. "Pseudo-spectral control of a novel oscillating surge wave energy converter in regular waves for power optimization including load reduction". *Ocean Engineering,* ***137***, pp. 352–366.
[18] Falnes, J., 2002. *Ocean Waves and Oscillating Systems: Linear Interactions Including Wave-Energy Extraction*. Cambridge University Press, Cambridge.
[19] Mei, C., 1989. *The Applied Dynamics of Ocean Surface Waves*. Advanced series on ocean engineering. World Scientific.
[20] Mehaute, B., 2013. *An Introduction to Hydrodynamics and Water Waves*. Springer Study Edition. Springer Berlin Heidelberg.